Modelling of the Mechanical Behaviour of Ultra-Fine Grained Titanium Alloys at High Strain Rates

N. Herzig[1], L.W. Meyer[1], D. Musch[1], T. Halle[1], V.A. Skripnyak[2], E.G. Skripnyak[2], S.V. Razorenov[3], L. Krüger[4]

[1] Chemnitz University of Technology, Materials and Impact Engineering, Germany
[2] Tomsk State University, Russia
[3] Russian Academy of Sciences, Institute of Problems of Chemical Physics, Chernogolovka, Russia
[4] Technical University Bergakademie Freiberg, Institut für Werkstofftechnik, Germany

Abstract

Results of numerical simulations of the mechanical behaviour of coarse grained and UFG titanium alloys under quasi-static uniaxial compression and plane shock wave loading are presented in this paper. Constitutive equations predict the strain hardening behaviour, the strain rate sensitivity of the flow stress and the temperature softening of titanium alloys with a range of grain sizes from 20 µm to 100 nm. Characteristics of the mechanical behaviour of UFG α and $\alpha+\beta$ titanium alloys in wide range of strain rates are discussed.

Keywords

Modelling, high strain rate, ultra-fine grain, material

1 Introduction

During the last decade a significant interest in production and processing of ultra-fine grained (UFG) materials arises. These materials usually show high strength and satisfactory plasticity at static loading. Designing of technology of mechanical forming of UFG metals needs constitutive equations of UFG materials with a good descriptive and predictive capability. The mechanical behaviour of UFG materials in a wide range of temperatures and strain rates is not adequately explored. Therefore, constitutive equations describing the plastic flow of such materials play an important role for computer simulations of mechanical forming processes.

The correct numerical simulation of shape changing during dynamic deformation requires the use of exactly determined physical parameters of constitutive equations. Constitutive models including grain size dependencies of metal alloys are presented e.g.

by Meyers et al. [1],[2] and Zerilli and Armstrong [3]. Khan et al. [4] modified the model of Johnson-Cook [5] by including a grain size dependent term. A suitable quantitative description of the mechanical behaviour of identical titanium alloys in coarse-grained and ultra-fine grained state is ensured by various values of model parameters. The material characteristics limit the opportunities of application of models for the prediction of the mechanical behaviour of ultra-fine grained titanium alloys under dynamic loading. The expected values of a static limit of flow of coarse grained and ultra-fine grained titanium alloys depend on the size of a grain allows receiving from Hall-Petch relation. However, obtaining realistic predictions of strain hardening and flow stress behaviour in a wide range of strain rates remains the issue of the day.

2 Materials

Constitutive equations were developed for α - titanium and $\alpha+\beta$ - titanium alloy Ti-6-22-22S (Ti-6Al-2Sn-2Zr-2Cr-2Mo-Si). The mechanical behaviour of the coarse grained and ultra-fine grained alloys were studied e.g. in [6] and [7]. The chemical composition of the alloys is shown in Table 1. The average grain size of coarse grained material is equal to 15 µm for α-Ti and 20 µm for Ti-6-22-22S. These alloys were processed by multi-axial compressions method. Hence, the average grain size of the specimens decreased to 300 nm.

Material	Al	Sn	Zr	Mo	Cr	Si	Fe	O	N	C
Ti-6-22-22S	5.75	1.96	1.99	2.15	2.10	0.13	0.04	0.082	0.006	0.009
α-Ti (VT1-0)	-	-	-	-	-	0.08	0.12	0.1	0.04	0.05

Table 1: *Chemical composition in wt.% of the grade titanium alloys*

3 Modelling

The conformity of the constitutive equations was studied by means of modelling of the mechanical behaviour of titanium alloys in a wide range of strain rates. Constitutive equations were used for simulation of the uniaxial deformation at Split Hopkinson Pressure Bar (SHPB) and the high velocity flyer plate impact. The system of constitutive equations describing the material deformation in Lagrange form can be written acc. eq. 1, where u_i is a component of particle velocity, E is the specific internal energy, ρ is a mass density, σ_{ij} is the component of the Cauchy stress tensor. Constitutive equations of the material deformation appropriate for high strain rate applications can be formulated by assuming, that the volumetric or dilatational response is governed by an equation of state (EOS), while the shear stress obeys a theory of plasticity. The stress in the material is expressed as the sum of the dilatational and deviatoric parts (eq. 2), where S_{ij} is the deviatoric part of the stress tensor, and p is the hydrostatic pressure defined to be positive in compression. S_{ij} is calculated by the eq. 3, where µ is the shear modulus, de_{ij}/dt and de^{p}_{ij}/dt are the deviatoric parts of the strain rate tensor.

$$\frac{1}{\rho}\frac{d\rho}{dt} = -\frac{\rho}{\rho_0}\nabla_i u_i\,,\ \rho\frac{du_i}{dt} = -\nabla_j \sigma_{ij}\,,\ \rho\frac{dE}{dt} = -\sigma_{ij}\frac{d\varepsilon_{ij}}{dt} \tag{1}$$

$$\sigma_{ij} = -p\,\delta_{ij} + S_{ij} \tag{2}$$

$$\frac{dS_{ij}}{dt} = 2\mu\left(\frac{de_{ij}}{dt} - \frac{de_{ij}^p}{dt}\right) \tag{3}$$

The components of S_{ij} at elastic deformation can be determined from eq. 3. The flow stress and strain relationship can be determined from a plasticity rule (eq. 4) or from an equation of plastic flow (eq. 5), where $\sigma_u = \sqrt{(3/2)\,S_{ij}S_{ij}}$, $d\dot{\varepsilon}_u^p = \sqrt{2/3\,d\dot{e}_{ij}^{(p)}d\dot{e}_{ij}^{(p)}}$, σ_s is the yield stress.

$$\sigma_u = \sigma_s(T, \varepsilon_u^p, d\varepsilon_u/dt) \tag{4}$$

$$\frac{de_{ij}^p}{dt} = \frac{3}{2}\frac{d\varepsilon_u^p}{dt}\frac{S_{ij}}{\sigma_u} \tag{5}$$

Specific features of mechanical properties of nanostructured materials are connected to distinctions of properties of matter in a crystalline phase of grains and properties of matter in the boundary of grains. The decrease of the mass density of nanostructured materials is caused by the increasing of defect density and relative volume of grain boundary phase. Significant changes of mass density of UFG titanium alloys take place at grain sizes less then 10 nm, when the relative volume of grain boundary areas of triple junction of grains sharply increases. The relative volume of grain boundary phase can amount to 20−25%, when the average sizes of a grain correspond to 10 − 20 nm. The elastic modulus of annealed UFG alloys with an average grain size exceeding 100 nm and coarse grained counterparts have no essential difference. At normal conditions the mass density of the titanium alloy Ti-6-22-22S is equal to 4.53 g/cm^3. The bulk modulus B and the shear modulus μ at the temperature T are calculated using eq. 6 and 7, where B_0 and μ_0 are the bulk and shear modulus at the room temperature T_0, γ is the Gruneisen factor, α is the coefficient of volumetric expansion.

$$B = B_0 + (T - T_0)\frac{\partial B}{\partial T}\,,\ \frac{\partial B}{\partial T} = -B_0\alpha\left(\frac{\partial B}{\partial p} - \gamma\right) \tag{6}$$

$$\mu = \mu_0 + (T - T_0)\left.\frac{\partial \mu}{\partial T}\right|_p + p\left.\frac{\partial \mu}{\partial p}\right|_T \tag{7}$$

The bulk modulus B_0 of Ti-6-22-22S alloy is equal to 105.0 GPa, $\partial B/\partial p$ is 4.37, and $\partial B/\partial T$ is –27 MPa/K. The shear modulus μ_0 is equal 46.2 GPa, $\partial\mu/\partial T$ is –2,7 MPa/K, $\partial\mu/\partial p$ 0.54, γ_0 corresponds to 1.23, α is equal to $3.3\cdot10^{-5}$ K^{-1} at 873 K and $1.4\cdot10^{-5}$ K^{-1} at 100 K. The bulk modulus and the shear modulus and their derivatives on pressure and temperature depend on the relative volume of the grain boundary phase (eq 8). Here, B and μ are the bulk and the shear modulus of nanostructured material, subscript ‘g’ corresponds to the grain boundary phase, subscript ‘cr’ corresponds to the crystalline phase, $C^{(g)}$ is the relative volume of the grain boundary phase.

$$B = B_g\, C^{(g)} + B_{cr}(1 - C^{(g)})\ ,\ \mu = \mu_g\, C^{(g)} + \mu_{cr}(1 - C^{(g)}) \tag{8}$$

The relative volume of a grain boundary phase of materials with a grain size of 300 nm and a thickness of the grain boundary region of ~5 nm is less then 0.1. The estimation of modulus leads to $B \sim 0.95 \cdot B_{cr}$ and $\mu \sim 0.95 \cdot \mu_{cr}$. The decrease of the bulk shear modulus of UFG alloys in comparison with the crystalline phase occurs, when grain sizes are smaller than 20 nm. Thus, the variation of the bulk and shear modulus of titanium alloys at grain sizes in the submicrometer range and down to 300 nm is not essential. Sound velocities of the materials can be calculated using eq. 9, where c_s, c_b and c_l are the shear, bulk and longitudinal sound velocities.

$$c_s = \sqrt{\frac{\mu}{\rho}}\ ,\ c_b = \sqrt{\frac{B}{\rho}}\ ,\ c_\ell = \sqrt{c_b^2 + \frac{4}{3}c_s^2} \tag{9}$$

At normal conditions the nominal longitudinal sound velocity of UFG titanium alloys is 6.01 km/s, and the bulk sound velocity is 4.87 km/s. The pressure in a wide range of compressibility can be described by the Mie-Gruneisen EOS (eq. 10, 11), where γ is the Gruneisen factor, E is a thermal part of the specific internal energy of material, $\xi = \rho_0/\rho$, B and B' are the bulk modulus of the material and its derivative on pressure, which is equal to 105 GPa and 4.4, respectively. The Grüneisen factor depends on the compressibility and is described by eq. 12, where γ_0 as a material constant is 1.1.

$$\mathrm{p} = \mathrm{p_c} + \gamma\, \mathrm{E} \tag{10}$$

$$\mathrm{p_c} = \frac{3}{2}\mathrm{B}(\xi^{-7/3} + \xi^{-5/3})\left(1 - \frac{3}{4}(4 - \mathrm{B}')(\xi^{-2/3} - 1)\right) \tag{11}$$

$$\gamma = \gamma_0(V/V_0) + (2/3)(1 - V/V_{0)}) \tag{12}$$

For the determination of the deviatoric part of the stress tensor S_{ij} the yield surface ought to be determined using eq. 4. The temperature dependent plastic flow stress relation in a wide range of plastic strains and strain rates can be described by the modified Johnson-Cook relation (eq. 13) or the Armstrong-Zerilli relation (eq. 14), or the relations of a micro-dynamical model (eq. 15-19).

$$\sigma_s = \left[A + B(\varepsilon_u^P)^n + k d_g^{-1/2}\right]\left[1 + C\ln\left(\dot{\varepsilon}_u / \dot{\varepsilon}_{u0}\right)\right]\left\{1 - \left(\frac{T - T_0}{T_m - T_0}\right)^m\right\} \tag{13}$$

$$\sigma_s = \sigma_{s0} + C_5\left(\varepsilon_u^p\right)^{n_1} + C_6 d_g^{-1/2} + C_2 \exp\left[-C_3 T + C_4 T \ln\left(\dot{\varepsilon}_u / \dot{\varepsilon}_{u0}\right)\right]. \tag{14}$$

Materials	A	B	n	k	C	m	$\dot{\varepsilon}_{u0}$
cg α-Ti	0.19	0.86	0.5	6.2	0.1643	0.7	1
UFG α-Ti	0.19	0.6	0.5	6.2	0.1613	0.7	1
cg Ti-6-22-22S	0.99	1.131	0.452	8.49	0.1284	0.7	1
UFG Ti-6-22-22S	0.99	1.131	0.452	8.49	0.1559	0.7	1

Table 2: *Constants of the modified Johnson-Cook model*

The material parameter of the modified Johnson-Cook and Armstrong-Zerilli equation are summarised in Table 2 and 3 for two different titanium alloys in coarse grained (cg) and ultra-fine grained (UFG) state.

Materials	σ_{s0}	C_6	C_2	C_3,	C_4	C_5	n_1
cg α-Ti	0.19	6.2	0.1843	0.000877	0.0004	0.86	0.5
UFG α-Ti	0.19	6.2	0.9298	0.000877	0.00015	0.6	0.5
cg Ti-6-22-22S	0.99	1.131	0.699	0.0024	0.01813	0.98	0.5
UFG Ti-6-22-22S	0.99	1.131	0.4464	0.0024	0.01681	1.01	0.5

Table 3: *Constants of the Armstrong-Zerilli model*

The strain hardening of titanium alloys associated with the accumulation of dislocations is described by eq. 15-17. The back stress σ_{bs} can be described using eq. 16, where α_1 is a phenomenological constant, b is the Burger's vector (for hcp titanium equal to 2.86 10-10 m), N the mobile dislocation density. The evolution of the dislocation density during deformation is described by eq. 17, where ξ=N/N_0, N_0 is the initial density of dislocations, K_0, K_1, and K_2 are phenomenological parameters of the material, q is a constant at the fixed temperature, t denotes the time, $\dot{\varepsilon}_0^p$ is equal to 1 s^{-1}. Using eq. 17 the increase of dislocation density during plastic deformation is taken into account. K_0 characterises the dislocation production during plastic flow, K_2 describes the annihilation of dislocations, K_1 characterises the emission of dislocations from the boundary of grains.

$$\sigma_s = \sigma_{s0} + \sigma_{bs} + C_6 d_g^{-1/2} + C_2 \, exp\left[-C_3 T + C_4 T \, ln\left(\dot{\varepsilon}_u / \dot{\varepsilon}_{u0}\right)\right] \tag{15}$$

$$\sigma_{bs} = \alpha_1 \mu b N^{1/2} \tag{16}$$

$$\frac{d\xi}{dt} = \frac{d\varepsilon_u^p}{dt}\left[K_0 + K_1\sqrt{\xi} - K_2\xi\left(\frac{1}{\dot{\varepsilon}_0^p}\frac{d\varepsilon_u^p}{dt}\right)^{-\frac{1}{q}}\right] \tag{17}$$

The approximation of the dependence of dislocation density versus effective plastic strain can be described using eq. 18, where N_0 is the initial density of dislocations, N^* is the largest density of dislocations, which is achieved in conditions of balance of processes of the generation and annihilation of dislocations, N' is the density of dislocations generated at dynamic loading, and G_1 is a material constant. Parameter N^* depends on temperature of the plastic deformation and is equal to ~10^{12} cm^{-2}. The initial dislocation density of UFG alloys produced by severe deformation methods is not less than ~10^9 cm^{-2}. The parameter $G_1/\mu b$ was determined to ~0.07 for coarse grained Ti-6-22-22S. Heterogeneous nucleation of dislocations under dynamic loading causes an increase of dislocation density. This rise of dislocation density is described by eq. 19, where n, η, σ_u^* are constants of the material, H is the Heaviside function, $\dot{\varepsilon}_{u0}^*$ is ~10^4 s^{-1}, and $\dot{\varepsilon}_{u0}$ =1.0 s^{-1}.

$$N = N^* - \left(N^* - N_0 - N'\right)\exp\left(-\tfrac{G_1}{\mu b}\varepsilon_u^p\right) \tag{18}$$

$$N' = \frac{1}{\eta}\left(\frac{\sigma_u}{\sigma_u^*} - 1\right)^n H(\sigma_u - \sigma_u^*)\, \mathrm{H}\left(\frac{\dot{\varepsilon}_u - \dot{\varepsilon}_{u0}^*}{\dot{\varepsilon}_{u0}}\right) \tag{19}$$

The critical stress σ_u^* of heterogeneous nucleation of dislocations depends on microstructure heterogeneity. Its value is equal to 1.45 GPa for coarse grained and 1.02 GPa for UFG Ti-6-22-22S. For α titanium σ_u^* is less than for $\alpha+\beta$ alloys and 0.63 GPa for coarse grained α-Ti and ~0.64 GPa for UFG alloy. Parameter η characterises the rate of dislocation density rise at shock loading. Its value depends on heterogeneity of microstructure. Eq. 15-19 allows the description of relaxation of the amplitude of an elastic precursor by means of taking into account of N'. It may be mentioned, that the constitutive equations (e.g. eq. 13, 14) do not allow the reception of a quantitative exact prediction of a relaxation of an elastic precursor for titanium alloys. The formation of dislocation cell substructures causes the transformation from the grain size to the average dislocation cell dimension. Fracture of titanium alloys at shock wave loading is described by the spall fracture model [7], where σ_1 is the principal stress, σ_{sp} is the spall strength and $\sigma_1 \geq \sigma_{sp}$. The spall strength of 4.7 GPa was used for simulation of spall fracture of UFG Ti-6-22-22S under shock wave loading. This value exceeds the spall strength (3.63-4.16 GPa) of its coarse grained counterpart [6]-[7].

4 Results

Variation of the grain sizes up to hundreds of nm causes a change of modulus of elasticity. Decrease of the bulk modulus leads to a change of shock adiabatic curve. The adiabatic compression curve received by eq. 10 and 11 is shown in Fig. 1. The solid curve corresponds to compression of polycrystalline titanium alloys. The dashed curve displays the calculated adiabat of UFG titanium with a grain size of 300 nm. Thus, coarse grained and UFG titanium alloys have no considerable difference in the Hugoniot adiabat. Both curves show a good correlation with experimental data in the range of intensity of dynamic compression up to 20 GPa. Differences in adiabatic curves of coarse-grained and nanostructured titanium alloy may appear at grain sizes of nanostructured alloys less than 50 nm. The influence of grain size on a plastic flow stress in a wide range of a strain rates is described by eq. 3-5 together with eq. 13-15. Fig. 2 shows the yield stress of α-Ti in a wide range of strain rates calculated using eq. 14.

Fig. 3 shows the yield stress of α-Ti in a wide range of strain rates calculated using eq. 13 and 14. The yield stress of coarse grained and UFG titanium alloys increases with the increasing strain rates in a range from 10^{-3} up to 10^{+6} s^{-1}. Eq. 13 allows receiving a suitable prediction of the yield stress at strain rates up to 10^4 s^{-1}. At grain sizes from 20 μm down to 50 nm the variation of the yield stress of titanium alloys in the range of strain rates from 10^{-4} to 10^6 s^{-1} can be described using eq. 14. Fig. 4 shows the calculated yield stress of α-Ti versus the average grain size at a strain rate of 10^{-3} s^{-1}.

It is necessary to note, experimental yield strength of titanium alloys with an average grain sizes from 5 µm down to 100 nm have a wide spacing of values, which is due to different manufacturing techniques for UFG materials. Fig. 5 and 6 show the strain rate sensitivity of the yield stress of UFG and coarse grained titanium alloys. The yield stresses at 0.2 % of plastic strain were used for estimation the strain rate sensitivity m. Factor m of UFG $\alpha+\beta$ titanium alloys increases at strain rates larger than 10^4 s^{-1}.

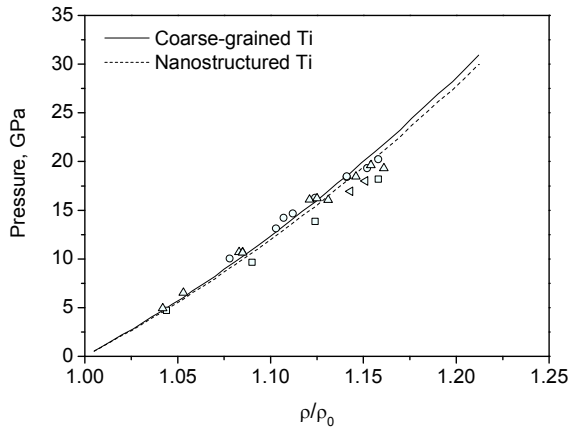

Figure 1: *Shock pressure versus relative mass density. Experimental data [9]*

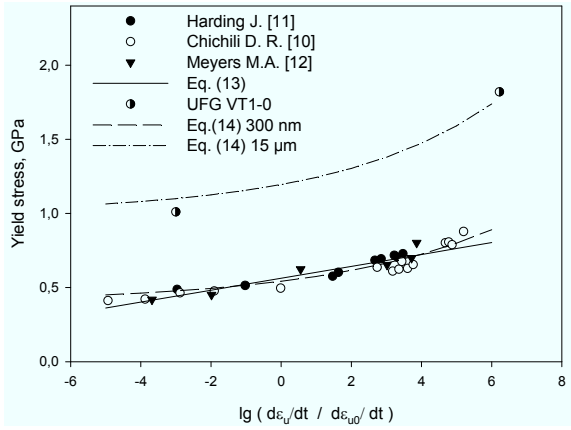

Figure 2: *Yield stress versus the logarithm of the normalized strain rate of α-Ti*

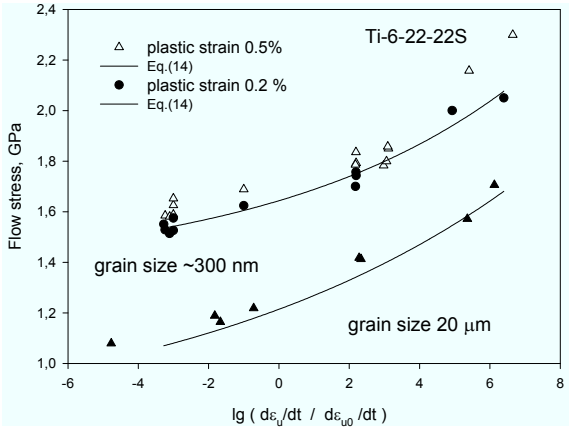

Figure 3: *Yield stress versus the logarithm of the normalized strain rate*

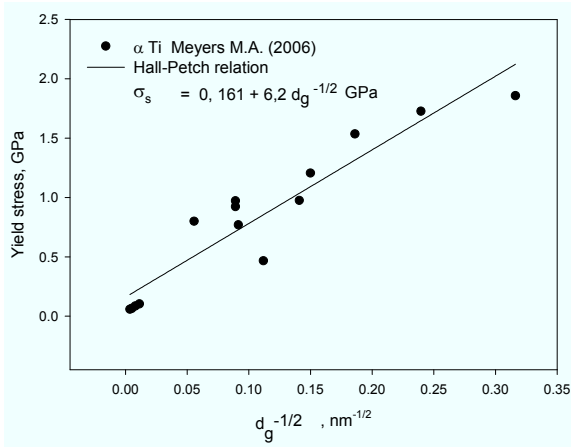

Figure 4: *Static yield stress of α titanium versus reciprocal square root of the grain size. Experimental data [1]*

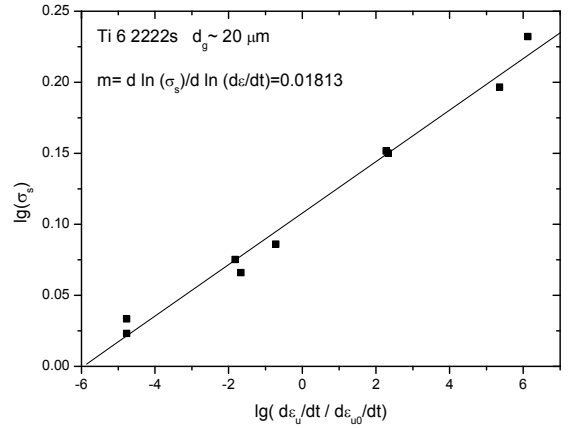

Figure 5: *Strain rate sensitivity of the yield stress of coarse-grained Ti-6-22-22S*

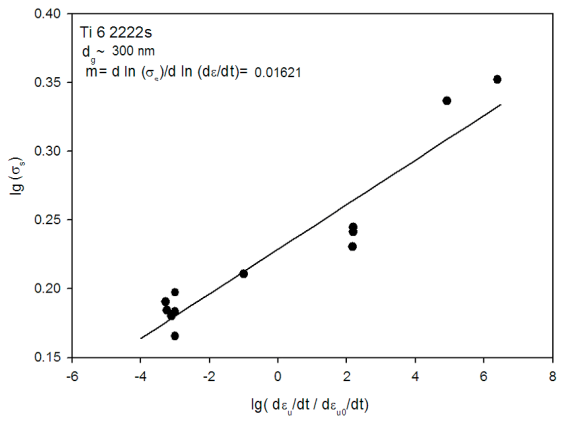

Figure 6*: Strain rate sensitivity of the yield stress of UFG Ti-6-22-22S*

Experimental results (Fig. 5 and 6) show that the strain rate sensitivity of the yield stress of UFG titanium alloys is not constant but rate dependent. Factor m of UFG titanium alloys increases in the investigated range of strain rates. This result differs from conclusions of [13] for materials with hcp, bcc and fcc lattice structure. The divergence in conclusions can be caused by using experimental data of flow stresses which correspond to different plastic strains. The strain rate sensitivity m strongly depends on the plastic strain.

Experimental and calculated yield stresses at plastic strains of 0.5% versus logarithm of strain rate are shown in Fig. 7. UFG alloys display a strong strain hardening at plastic strains up to 1% in comparison with coarse grained materials. Results of numerical simulations of strain hardening of UFG and coarse grained Ti-6-22-22S alloy are shown in Fig. 8. Strain hardening of UFG titanium alloys depends on strain rate. This effect was neglected by constitutive equations of Johnson-Cook [5] and Zerilli-Armstrong [3]. The variation of the factor B of the eq. 13 or the factor C_5 of the eq. 14 give the possibility to have a good quantitative accordance of the calculated strain hardening with experimental data. Sharp increase of dislocation density at dynamic loads can be the reason of changing in the strain hardening rate.

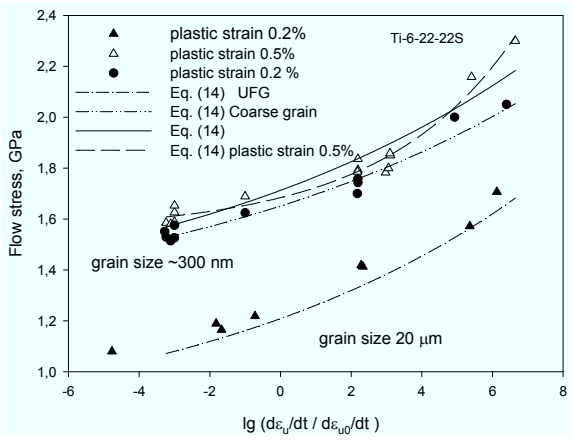

***Figure 7**: Yield stress versus the logarithm of the normalized strain rate*

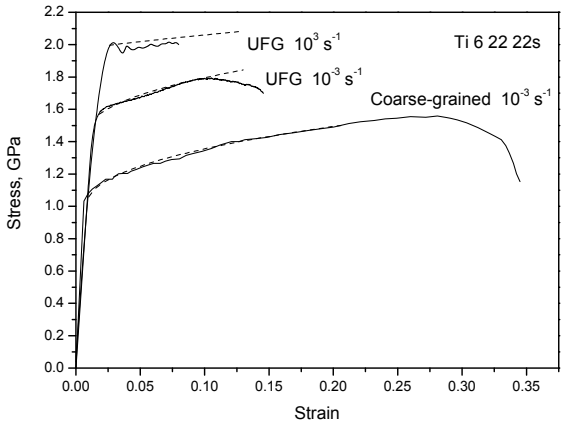

***Figure 8:** Stress versus strain of Ti-6-22-22S titanium alloy. Solid curves correspond to experimental data. Dashed curves are results of calculation*

Eq. 16-19 describe the flow stress dependence on strain rate and plastic strain. Results of numerical simulations of the deformation of α-Ti are shown in Fig. 9. The Autodyn code was used for the simulation of plane shock wave loading of coarse-grained and UFG material. Eq. 14-15 were used for describing of mechanical behaviour of Ti-6-22-22S alloy.

The results of computer simulations of the time history of the free surface velocity under plane shock wave loading are shown in Fig. 10. A good correlation of calculated shock wave amplitudes and duration of shock pulses with experimental data confirms the applicability of the equation of state (eq. 10-12) and constitutive equations of plastic flow (eq. 3-5 and 13-19) for description of the mechanical behaviour of UFG alloys. Fig 10 shows a suitable coincidence of predicted spall strength with experimental results. It can be seen that higher free surface particle velocities can be measured for higher impact

velocities and, hence, a higher spall strength can be found. There, an impact velocity of 660 m/s corresponds to shock pulse amplitudes of ~5-6 GPa and 1250 m/s to ~10 GPa, respectively. The good qualitative consent of the structures of calculated shock pulses after spall fracture of the ultra fine-grained titanium shows that the fracture model suggested in [7] is applicable for prediction of the failure under dynamic impacts.

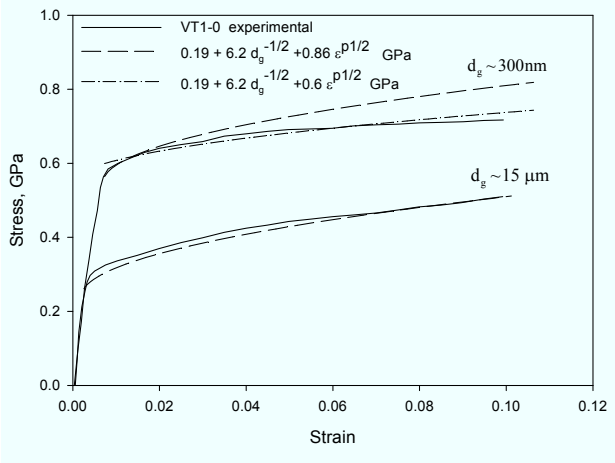

Figure 9: *Stress versus strain of α-titanium (VT1-0) at strain rate 10^{-3} s^{-1} [9]*

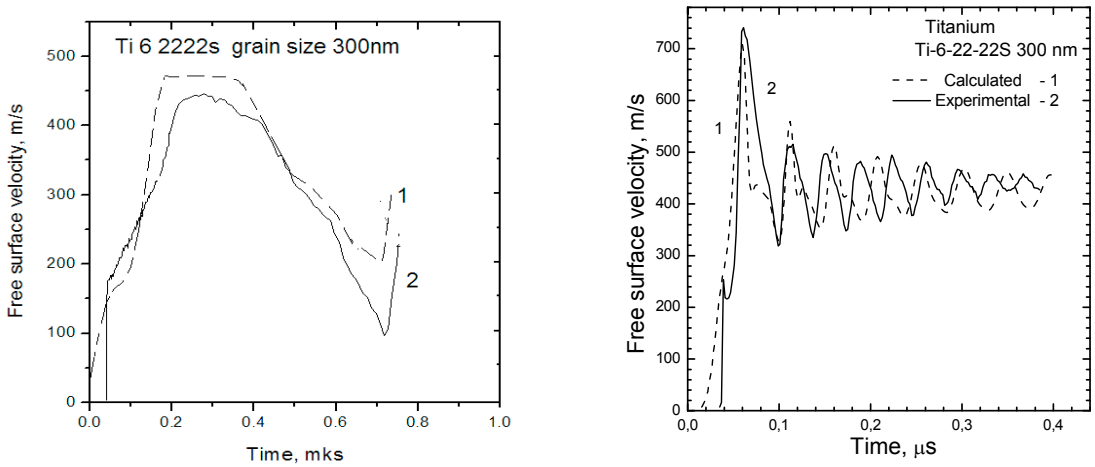

Figure 10: *Calculated (1) and experimental (2) time history of free surface velocity under plane shock wave loading. left) numerical simulation of 660 m/s impact of 2 mm aluminium impactor on 6.36 mm specimen of UFG Ti-6-22-22S. Velocity of impact is 660 m/s. right) results of simulation of impact of 0.12 mm aluminium impactor on 0.835 mm specimen. Velocity of impact is 1250 m/s*

5 Conclusions

From our work the following conclusions can be drawn:

1. The mechanical behaviour of coarse grained and UFG titanium alloys is strongly dependent on strain and strain rate.

2. Thermally activated flow stress behaviour was found for the titanium alloys up to strain rates of 10^6 s^{-1}. No drag effects were measured within the tested range of strain rates.
3. Non-linear constitutive equations have been developed for describing of the mechanical behaviour of UFG and coarse grained titanium alloys. Eq. 13-15 can be used to describe the plastic flow stress behaviour of UFG alloys as a function of the grain size, strain rate, plastic strain, and temperature.
4. Results of computer simulations show a good qualitative consent with experimental data. Simulated free surface velocity profiles can be used for further evaluation procedures.
5. A simple model of the spall fracture is suitable for prediction of the dynamic spall failure of UFG titanium alloys at shock impact loading.

References

[1] *Meyers, M.A.; Mishra, A.; Benson, D.J.:* Mechanical properties of nanocrystalline materials. Progress in Materials Science, 51 (2006), 427–556.

[2] *Meyers, M.A.; Vohringer, O.; Lubarda, V.A.:* The onset of twinning in metals: a constitutive description. Acta mater. 49 (2001), 4025–4039.

[3] *Zerilli, F.J.; Armstrong, R.W.:* Dislocation-mechanics-based relations for material dynamics calculations. J. Appl. Phys. 61 (1987), 1816-1825.

[4] *Khan, A.S.; Suh, Y.S.; Kazmi, R.:* Quasi-static and dynamic loading responses and constitutive modeling of titanium alloys. Int. J. of Plasticity 20 (2004), 2233–224.

[5] *Johnson, G.R.; Cook, W. H.:* A constitutive model and data for metals subjected to large strains, high strain rates and high temperatures. Proc. of the 7th Int. Symp. on Ballistics. Hague, Netherlands. 1983, 541-547.

[6] *Skripnyak V.A., Skripnyak E.G.* Shear strength of nanocrystalline and UFG materials under shock wave loading. Physical mesomechanics, 7 (2004), 297-300.

[7] *Krüger L., Kanel G.I., Razorenov S.V., Meyer L.W., Bezrouchko G.S.:* Yield and strength properties of the Ti-6-22-22S alloy over a wide strain rate and temperature range. In: Shock compression of condensed matter. 2002. 1327-1331.

[8] *Estrin Y.* Unified constitutive laws of plastic deformation. / Ed. by Krausz A.S., Krausz K. New York: Academic Press; 1996. 69.

[9] *Trunin R. F., Belyakova M. Yu., Zhernokletov M. V., Sutulov Yu. N.* Shock compression of metallic alloys. Izv. Akad. Nauk SSSR. Physics of the Solid Earth, 2 (1991), 99–106.

[10] *Chichili D. R. , Ramesh K. T., Hemker K. J.* The high strain-rate response of alpha-titanium: experiments, deformation mechanisms and modelling. Acta mater. 46 (1998), 1025-1043.

[11] *Harding J.* The temperature dependence and strain rate sensitivity of alpha-titanium. Arch. Mech. 27 (1975), 715- 732.

[12] *Meyers M.A. et al.* Evolution of microstructure and shear-band. Progress in Materials Science, 51 (2006), 427–556.

[13] *Kumar K.S., Van Swygenhoven H., Suresh S.* Mechanical behaviour of nanocrystalline metals and alloys. Acta Mater. 51 (2003), 5743–5774.